RSC Advances

PAPER

View Article Online
View Journal | View Issue



Cite this: *RSC Adv.*, 2024, **14**, 5926

# Synthesis, computational chemical study, antiproliferative activity screening, and molecular docking of some thiophene-based oxadiazole, triazole, and thiazolidinone derivatives†

Amna S. Elgubbi, [a] Eman A. E. El-Helw, *[b] Abdullah Y. A. Alzahrani[c] and Sayed K. Ramadan [b]

Thiophene-2-carbohydrazide was used in this study to produce some thiophene-containing oxadiazole, triazole, and thiazolidinone derivatives through reactions with various carbon-centered electrophiles. Besides, the hydrazone obtained was allowed to react with mercaptoacetic acid and acetic anhydride to construct thiazolidinone and oxadiazole derivatives. The results of computational chemical study and outcomes of the experiments were in good agreement. The *in vitro* antiproliferative activity of the produced compounds was examined against two human cell lines namely, breast adenocarcinoma (MCF7) and colon cancer (HCT116) cell lines using doxorubicin as a reference anticancer agent. The produced hydrazones and spiro-indolin-oxadiazole derivatives were the most potent against the two cancer cell lines. The molecular docking was conducted to demonstrate the binding energies of produced substances toward human carbonic anhydrase IX (CA IX) protein. The binding energies of these ligands were near to that of the co-crystallized ligand (9FK). Compound **11b** exhibits a binding energy of −5.5817 kcal mol$^{-1}$, indicating tight binding to some key nucleobases and amino acids of CA IX protein, while compound **11a** displays a higher binding energy compared to the reference ligand (9FK). This suggests that compounds **11b** and **11a** display a notably strong binding affinity towards the human carbonic anhydrase IX (CA IX) protein. ADME profiles of the potent compounds including physicochemical characteristics, lipophilicity, and drug-likeness were predicted.

Received 16th October 2023
Accepted 7th February 2024

DOI: 10.1039/d3ra07048d

rsc.li/rsc-advances



## Introduction

Thiophene and its derivatives are a significant class of heterocyclic compounds which exhibit interesting applications in the field of medicinal chemistry. A thiophene core is also present in several naturally-occurring products and numerous pharmacologically-active skeletons.[1,2] Thus, good antimicrobial effects were shown by thiophene derivatives against various microbial infections.[3] It is noteworthy that, many commercially-available anticancer agents contain a thiophene nucleus and exert their effects through multiple pathways involved in cancer.[4–6] Therefore, the evaluation of toxicity of the novel chemicals is important to develop new control recommendations. In turn, several commercially available drugs include a thiophene nucleus such as articaine, duloxetine, dorzolamide, thenoyltrifluoroacetone, rivaroxaban, canagliflozin, tipepidine, timepidium bromide, tioconazole, citizolam, sertaconazole nitrate, and benocyclidine (*cf.* Fig. 1).

On the other hand, the acid hydrazides have been easily converted into hydrazones, oxadiazoles, triazoles, and various heterocycles.[7–10] Among the hydrazides, 2-thienohydrazides have received extensive attention due to the biological effects of thiophene moiety which were recognized and practically applied in herbicides,[11] fungicides,[12] and several agents.[13]

Otherwise, it was shown that thiosemicarbazide derivatives provide various functionality through nucleophilic and electrophilic centers. In fact, they served as a crucial intermediate for the synthesis of many useful heterocyclic compounds with five- and six-membered rings.[14,15] Noteworthy, some oxadiazoles, triazoles, and thiazolidinones showed good *in vitro* antiproliferative activities against a wide range of human tumor cell lines, with the $GI_{50}$ in the micromolar to the sub-micromolar range.[16–19] Further, 1,3,4-oxadiazoles are found in many molecules with antitumor activity and known as bio-isosteres of esters and amides that can contribute interesting pharmacokinetic properties due to the presence of N=C–O linkage, which rises lipophilicity and affects

[a]*Chemistry Department, Faculty of Science, Misurata University, 2478, Misurata, Libya*

[b]*Chemistry Department, Faculty of Science, Ain Shams University, Cairo, 11566, Egypt. E-mail: eman.abdelrahman@sci.asu.edu.eg*

[c]*Chemistry Department, Faculty of Science and Arts, King Khalid University, Mohail Assir, Abha, Saudi Arabia*

† Electronic supplementary information (ESI) available: All spectroscopic data can be found in supplemental files. See DOI: https://doi.org/10.1039/d3ra07048d

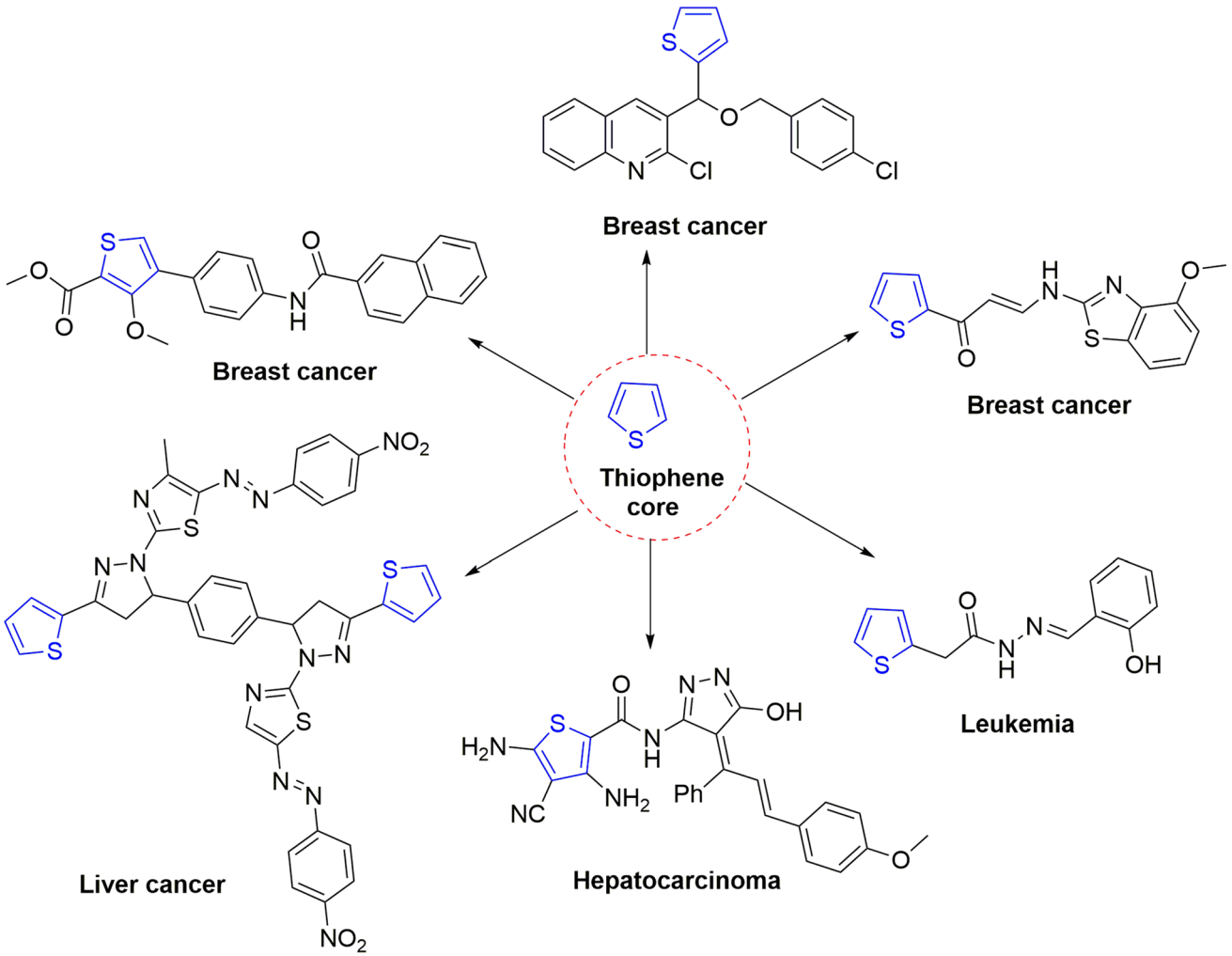


Fig. 1 Some clinical drugs bearing thiophene scaffolds as anticancer agents.

the ability of the drugs to reach molecular targets by transmembrane diffusion.[20] In recent years, 4-thiazolidinone derivatives have become a promising area of research with antitumor activity on leukemia, renal, melanoma, colon, lung, CNS, prostate, and breast cancer cell lines.[21] These nitrogen heterocycles constitute the pharmacophore moieties of various molecules with different biological activities, including antitumor activity due to their ability to bind with target proteins.[22]

Continuing our studies on diverse heterocyclic systems with different pharmacological properties,[23–30] the biological activities of these pharmacophores led us to design and synthesize of some lead thiophene-bearing heterocycles utilizing thiophene-2-carbohydrazide **1** aiming to enhance their *in vitro* antiproliferative activity, besides their computational chemical approach, molecular docking, and modeling pharmacokinetics studies.

## Rationale and design

Thiophene has been recognized as a crucial scaffold due to its presence in many pharmacologically-active compounds. In our pursuit to develop prospective antiproliferative compounds, inspiration was drawn from thiophene's pharmacophoric features, which have shown efficacy in treating breast cancer, leukemia, hepatocarcinoma, and others (*cf.* Fig. 2). To design and synthesize a series of some 2-substituted thiophene derivatives, the fundamental pharmacophoric features of thiophene were kept while integrating heterocyclic and side chain moieties, which are as follows: (i) a planar aromatic core (chromophore), which has been associated with antiproliferative activity, was retained in the design, (ii) the linker was modified by incorporating heteroatoms like oxygen (O), sulfur (S), and nitrogen (N) in order to establish more hydrogen bonds during interaction with tumor proteins, (iii) to boost the antiproliferative activity of the compounds, cores of pyrazole, chromone, oxadiazole, and indole were integrated into the design, which have been found to have promising effects in this view, (iv) some different aldehyde derivatives were opted to promote enhanced interactions with the target proteins. By combining these features, this work intended to prepare some 2-substituted thiophene derivatives with

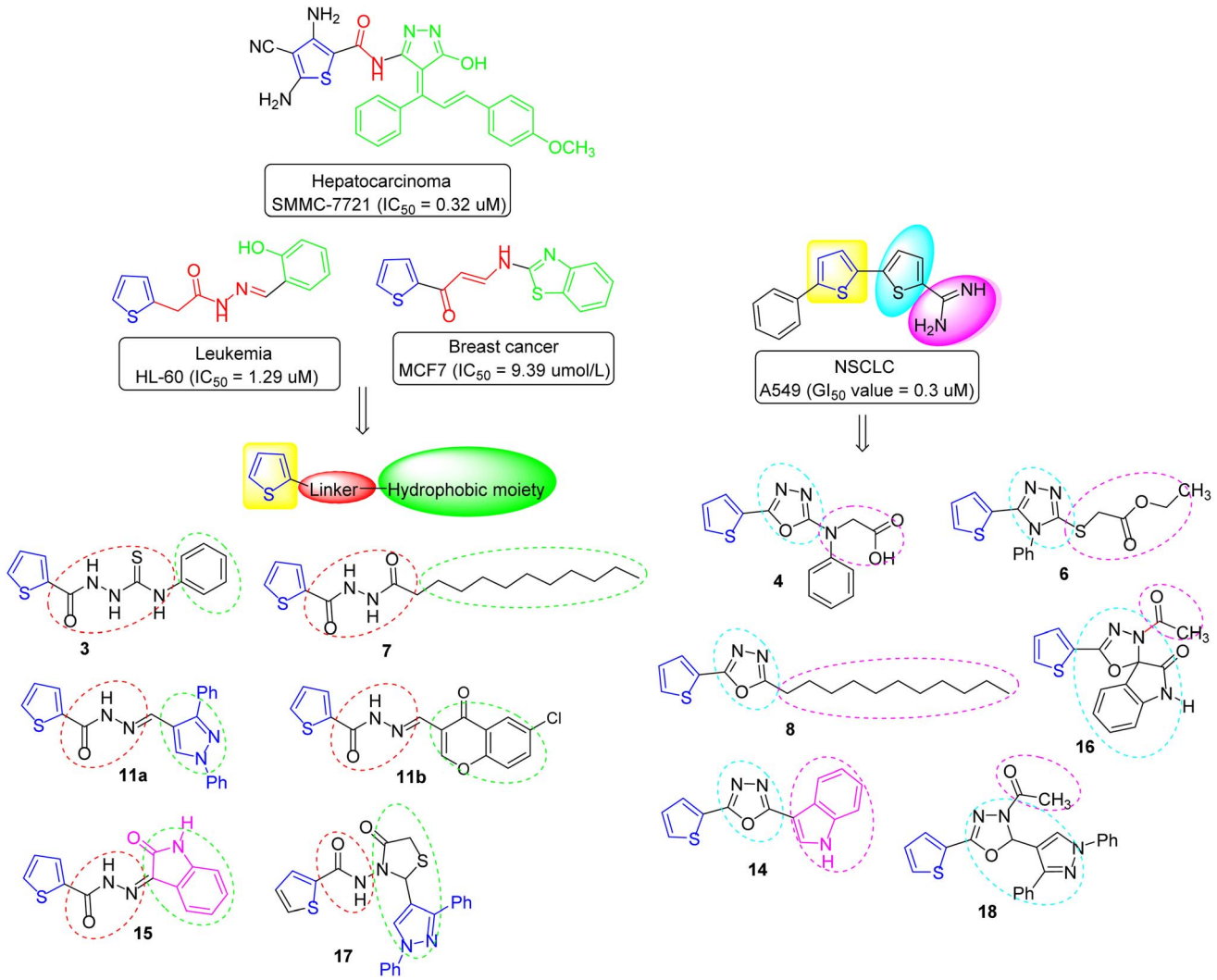


Fig. 2 Rationale and design of the chemical structures of some anticancer agents (bearing thiophene nucleus) and the target derivatives.

improved antiproliferative effects. This rationale-based design holds the potential for the development of promising antiproliferative compounds with the desired therapeutic effects (*cf.* Fig. 2).

## Results and discussion

### Chemistry

The building block synthon, thiphene-2-carbohydrazide **1** (ref. 31) was utilized for the construction of some thiophene-based heterocyclic systems.[32] Thus, the hydrazide **1** reacted with phenyl isothiocyanate **2** in boiling ethanol to give thiosemicarbazide **3** (ref. 33) as white crystals (Scheme 1). The absorption bands of NH, C=O, and C=S were shown in the IR spectrum of compound **3** (*cf.* Experimental). The oxadiazole derivative **4** was produced through treating compound **3** with chloroacetic acid in boiling *N*,*N*-dimethylformamide (DMF) using triethylamine ($Et_3N$) as a base. A broad absorption for the carboxylic-OH moiety of compound **4** was displayed in its IR spectrum in addition to the carbonyl absorption.

The formation of oxadiazole **4** could be distinctly explained *via* 1,5-*exo*-trig intramolecular cyclization of **3** by removing gaseous hydrogen sulfide molecule, as detected by the change in color of lead acetate paper into black, followed by a nucleophilic attack of –NH on methylene group of chloroacetic acid *via* $S_N2$ route (Scheme 2).

Otherwise, combining compound **3** with ethyl chloroacetate in boiling acetic acid including anhydrous sodium acetate did not give the thiazolidinone **5**, but afforded the triazole **6** as colorless needles (Scheme 1). The IR spectrum of compound **6** lacked NH absorption band and displayed the absorption band for ester carbonyl group. Further, its mass spectrum displayed the molecular ion peak at *m*/*z* 345 (37%), a fragment peak at *m*/*z* 272 (49%) attributable to loss of $–COOC_2H_5$ radical, and the base peak at *m*/*z* 77 (100%), in addition to some abundant peaks.

Perhaps, the formation of triazole **6** could be demonstrated *via* 1,5-*exo*-trig intramolecular cyclization of thiosemicarbazide derivative **3** by eliminating water molecule followed by a nucleophilic attack of –SH on $–CH_2Cl$ group of ethyl chloroacetate *via* $S_N2$ route (Scheme 3).

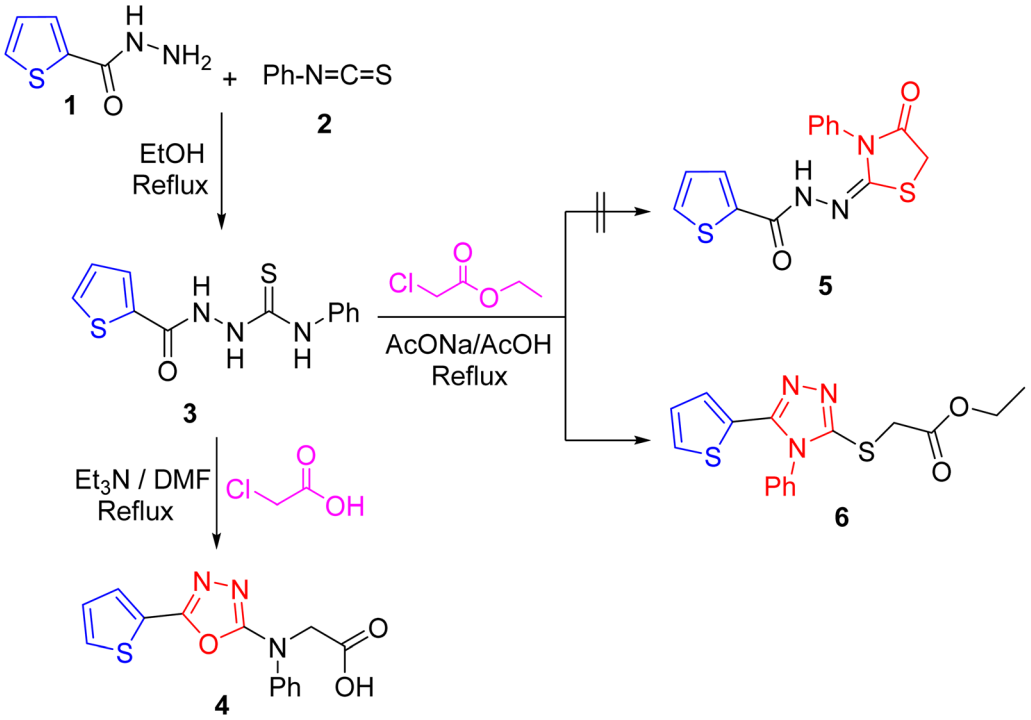


Scheme 1 Synthesis of oxadiazole **4** and triazole **6** derivatives.

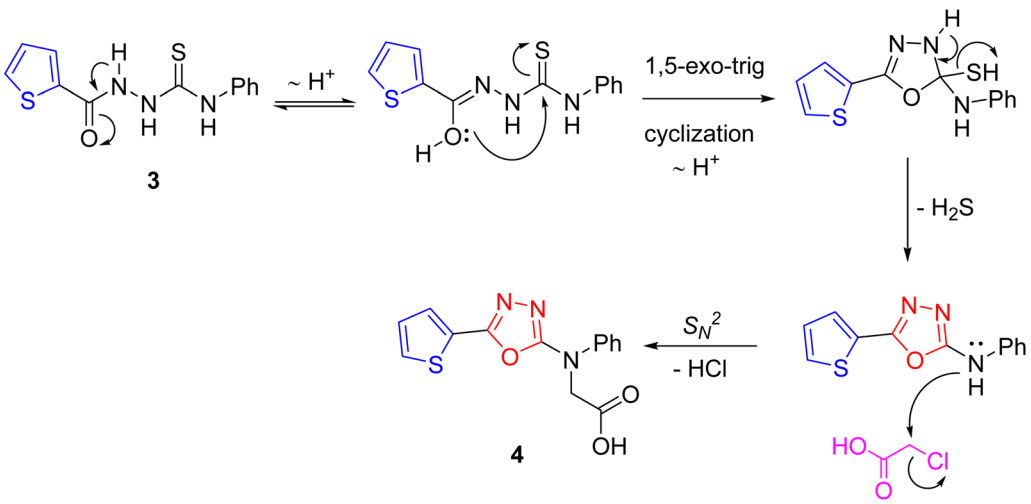


Scheme 2 A plausible pathway for the formation of oxadiazole derivative **4**.

In turn, reaction of hydrazide **1** with dodecanoyl chloride in pyridine afforded the corresponding dodecanoyl hydrazide **7** which was transformed into the oxadiazole **8**, *via* elimination of water molecule, through heating with phosphorous oxychloride (Scheme 4). In the IR spectrum of compound **7**, the absorption peaks of NH and C=O moieties were displayed. Further, its mass spectrum displayed the molecular ion peak as well as other abundant peaks (*cf.* Experimental). Treatment of the hydrazide **1** with arylidine malononitrile **9a** and **9b** in boiling 1,4-dioxane furnished the corresponding thiophene-2-carbohydrazones **11a** and **11b** instead of the enaminonitrile **10a** and **10b**.

The IR spectrum of compound **11a** and **11b** disclosed NH and C=O absorptions. Also, $^1$H NMR spectrum of hydrazone **11a** offered signals for an exchangeable NH singlet, methine CH=N proton singlet, and C5–H (of pyrazole moiety) singlet. Moreover, its correct molecular ion peak was appeared in its mass spectrum. The formation of hydrazones **11a** and **11b** might be demonstrated *via* aza-Michael addition of primary amino group on β-carbon of activated nitrile followed by rearrangement to eliminate malononitrile molecule (*cf.* Scheme 5). The hydrazones **11a** and **11b** were also obtained through treating the hydrazide **1** with the aldehydes **12a** and **12b** (*cf.* Scheme 4).[34]

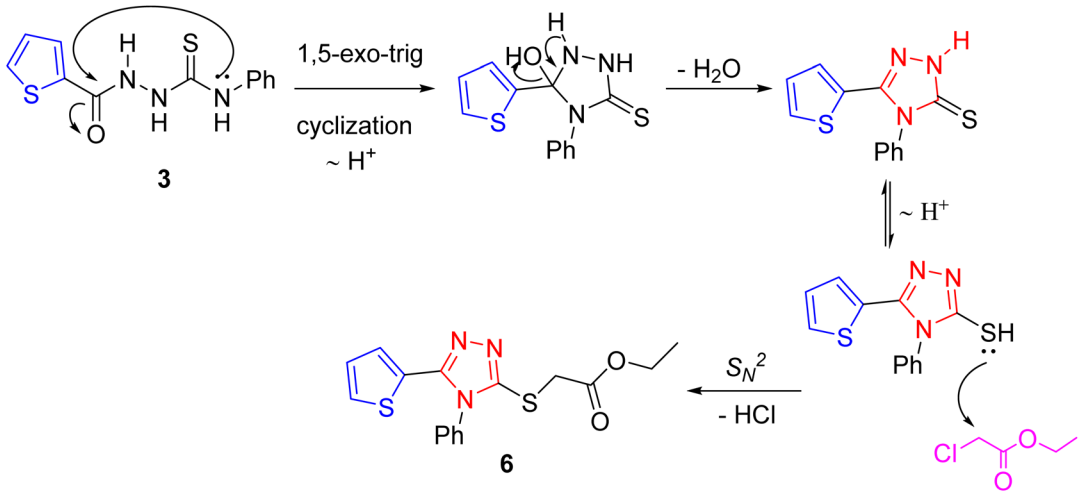


Scheme 3 A suggested pathway for the formation of triazole derivative **6**.

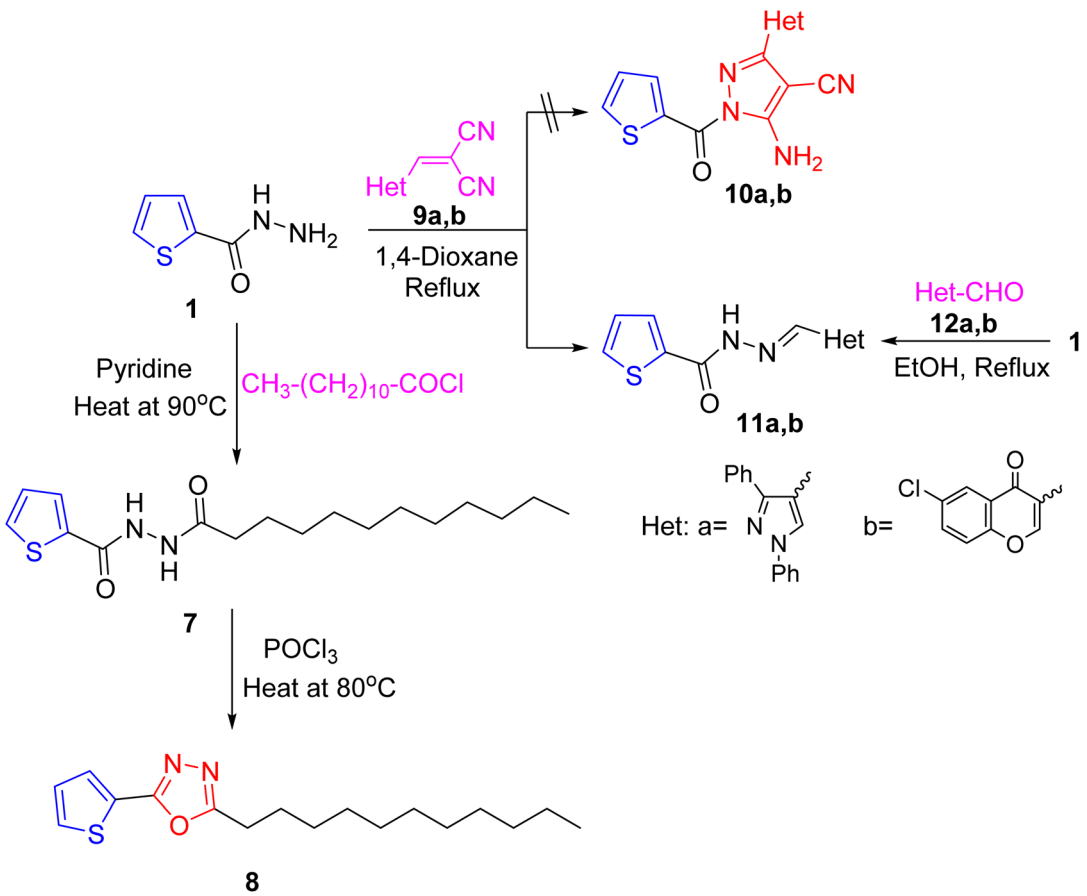


Scheme 4 Synthesis of compounds **7**, **8**, and **11a** and **11b**.

On the other side, the oxadiazole **14** was produced by condensation of hydrazide **1** with 3-formylindole in boiling 1,4-dioxane *via* the hydrazone intermediate **13** (Scheme 6). The lack of carbonyl absorption in the IR spectrum of compound **14** corroborated the 1,5-*endo* trig cyclization process. Further in its $^1$H NMR spectrum, one exchangeable singlet signal appeared in the downfield region attributable to NH proton of the indolyl moiety. While condensation of hydrazide **1** with indolin-2,3-dione afforded the hydrazone **15** (ref. 35) which was converted into the spiro compound **16** through heating with acetic anhydride (*cf.* Scheme 6). Spectroscopically, the IR spectrum of compound **16** offered

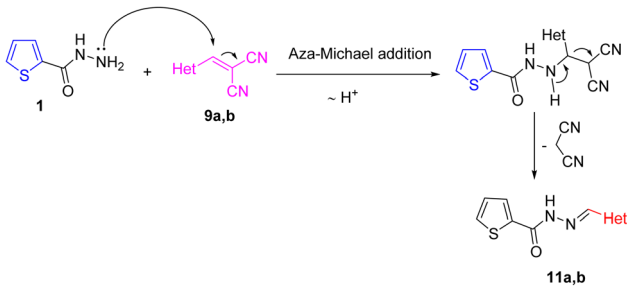


Scheme 5 A suggested pathway for the formation of hydrazone **11a** and **11b**.

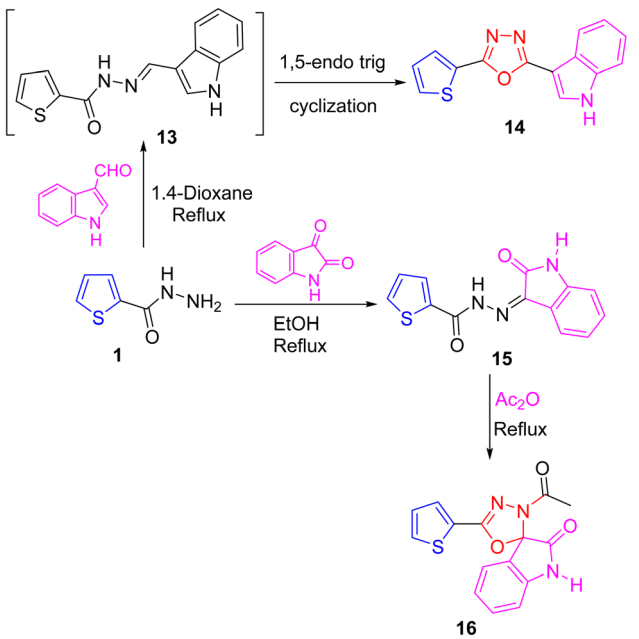


Scheme 6 Condensation of hydrazide **1** with 3-formylindole and indolin-2,3-dione.

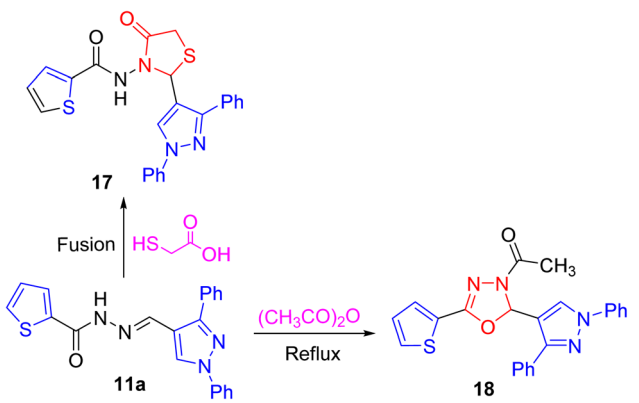


Scheme 7 Reactions of hydrazone **11a** with mercaptoacetic acid and acetic anhydride.

absorption bands for the two carbonyl functionalities. Also, in its $^1$H NMR spectrum chart, a singlet signal appeared in the downfield region corresponding to NH proton, and a singlet

Table 1 Energy level distribution of frontier orbitals and global reactivity indices[a]

| Compd | *E | $E_{HOMO}$ (eV) | $E_{LUMO}$ (eV) | $\Delta E$ (eV) | $\mu$ (Debye) | $\eta$ (eV) | $\varsigma$ (eV$^{-1}$) | $\mu_o$ (eV) | $\omega$ (eV) | $n$ (eV$^{-1}$) | $I_p$ (eV) | EA (eV) | $x$ (eV) |
|---|---|---|---|---|---|---|---|---|---|---|---|---|---|
| **3** | 11.606 | −6.646 | 0.350 | 6.996 | −0.054 | 3.498 | 0.286 | −3.50 | 1.75 | 0.571 | 6.646 | 0.350 | 3.498 |
| **4** | 30.915 | −6.423 | 0.077 | 6.500 | 3.668 | 3.250 | 0.307 | −3.25 | 1.62 | 0.617 | 6.423 | 0.077 | 3.250 |
| | 39.628 | −5.638 | −0.193 | 5.445 | −4.141 | 2.722 | 0.367 | −2.91 | 1.55 | 0.645 | 5.638 | 0.193 | 2.915 |
| **6** | 59.541 | −5.845 | 0.351 | 6.196 | 2.538 | 3.098 | 0.323 | −3.10 | 1.55 | 0.645 | 5.845 | 0.351 | 3.098 |
| **7** | 9.135 | −8.043 | 0.582 | 8.625 | −10.369 | 4.312 | 0.232 | −4.31 | 2.15 | 0.465 | 8.043 | 0.582 | 4.312 |
| **8** | 28.623 | −7.167 | 2.962 | 10.129 | 5.101 | 5.064 | 0.197 | −5.06 | 2.53 | 0.395 | 7.167 | 2.962 | 5.064 |
| | 67.043 | −7.222 | −1.071 | 6.151 | 3.532 | 3.075 | 0.325 | −4.15 | 2.80 | 0.357 | 7.222 | 1.071 | 4.146 |
| | 63.121 | −7.491 | −3.967 | 3.524 | 8.232 | 1.762 | 0.567 | −5.73 | 9.32 | 0.107 | 7.491 | 3.967 | 5.729 |
| **11a** | 35.219 | −7.040 | −1.601 | **5.439** | −3.718 | 2.719 | 0.368 | −4.32 | 3.43 | 0.291 | 7.040 | 1.601 | 4.320 |
| **11b** | 32.020 | −7.141 | −4.014 | **3.127** | −1.591 | 1.563 | **0.640** | −5.58 | 9.96 | 0.100 | 7.141 | 4.014 | 5.577 |
| | 20.592 | −7.181 | −0.798 | 6.383 | −3.625 | 3.191 | 0.313 | −3.99 | 2.49 | 0.402 | 7.181 | 0.798 | 3.989 |
| **14** | 29.137 | −6.736 | −0.448 | 6.288 | 5.179 | 3.144 | 0.318 | −3.59 | 2.05 | 0.488 | 6.736 | 0.448 | 3.592 |
| **15** | 21.489 | −7.694 | −3.162 | **4.532** | −1.610 | 2.266 | 0.441 | −5.43 | 6.50 | 0.154 | 7.694 | 3.162 | 5.428 |
| **16** | 32.689 | −7.279 | −0.009 | 7.270 | 4.297 | 3.635 | 0.275 | −3.64 | 1.82 | 0.549 | 7.279 | 0.009 | 3.644 |
| **17** | 37.032 | −7.626 | −1.082 | 6.544 | 0.409 | 3.272 | 0.305 | −4.35 | 2.89 | 0.346 | 7.626 | 1.082 | 4.354 |
| **18** | 38.957 | −7.580 | −1.081 | 6.499 | −0.776 | 3.249 | 0.308 | −4.33 | 2.88 | 0.347 | 7.580 | 1.081 | 4.330 |
| Dox. | 67.785 | −9.189 | −7.149 | 2.040 | 3.954 | 1.020 | 0.98 | −8.17 | 32.72 | 0.030 | 9.189 | 7.149 | 8.169 |

[a] Dox.: doxorubicin, *$E$: minimized energy (kcal mol$^{-1}$), $\mu$: dipole/dipole, $\eta$: global hardness, $\varsigma$: global softness, $\mu_o$: chemical potential, $\omega$: global electrophilicity index, $n$: nucleophilicity index, $I_p$: ionization potential, EA: electron affinity, $x$: electronegativity.

signal existed in the upfield region corresponding to the methyl protons.

In turn, thiazolidinone derivative **17** was obtained through treating the pyrazolylhydrazone **11a** with mercaptoacetic acid under fusion conditions. It was fortunate that, boiling the hydrazone **11a** with acetic anhydride afforded oxadiazole derivative **18** as yellow crystals (*cf.* Scheme 7). In IR spectrum of compound **18**, the amide carbonyl absorption appeared. Besides, its $^1$H NMR spectrum displayed a singlet signal for C5–H pyrazole, a singlet signal for C2–H oxadiazole at, and a singlet signal for methyl protons. The mass spectra of the produced compounds supported the assigned structures (*cf.* Experimental).

## Computational chemical study

**Density functional theory (DFT) study.** DFT was used to optimize the molecular structures of the produced compounds employing Materials Studio 6.0 (MS 6.0) software from Accelys, Inc. DMol3 was utilized to perform the DFT calculations applying hybrid *B3LYP* functional and *3-21G* basis set. DFT was utilized to identify the electrophilic and nucleophilic centers and interpret the courses of reactions. It is known as optimization when the molecular structures of produced substances are superior to those created to a stable geometry. Thiophene derivatives' geometry was gradually optimized, and their energy was continuously decreased until the fluctuations in the molecule's energy were minimized. As a result, the structure's energy was moved to a stationary point. The electrophilic attack centers are characterized by the HOMO areas of maximum electron density, whereas the nucleophilic attack sites are denoted by the LUMO regions. It is generally known that high $E_{HOMO}$ values are likely to signify a molecule's strong propensity to donate electrons.

Due to the low energy needed to remove an electron from the last occupied orbital, low values of the energy gap ($\Delta E = E_{LUMO} - E_{HOMO}$) will exhibit strong inhibition efficiency.[29,36–38] The optimization of the structure of intermediate that reacted to produce the final product is profiled by DFT based on quantum chemical computing.

To demonstrate how thiophene-2-carbohydrazide **1** reacted with some reagents to produce compounds **3–18**, we used DFT simulation. Analytical and spectral data supported the chemical structures. The calculations of produced compounds can be performed using the DFT approach to calculate quantum chemical properties (*cf.* Table 1). A good explanation for the synthetic compounds agreed with the dipole moments for thiophene derivatives. The optimized, HOMO, and LUMO structures of compounds **3–18** were drawn using ChemBio3D Ultra 14.0 and depicted in Fig. 3 (*cf.* ESI†). HOMOs are dispersed around thiophene unit in compound **3** and LUMOs are focused on benzene moiety.

The calculated $\Delta E$ was compared with theoretical reference data based on the corresponding experimental results in gas phase reaction. With $\Delta E$ being a criterion, three most typical and popular exchange-correlation functionals *e.g.*, PW91 were systematically compared in terms of the typical synthesis in gas phase *via* reactions of thiophene-2-carbohydrazide **1** with some carbon-electrophilic centers. The present work provides general

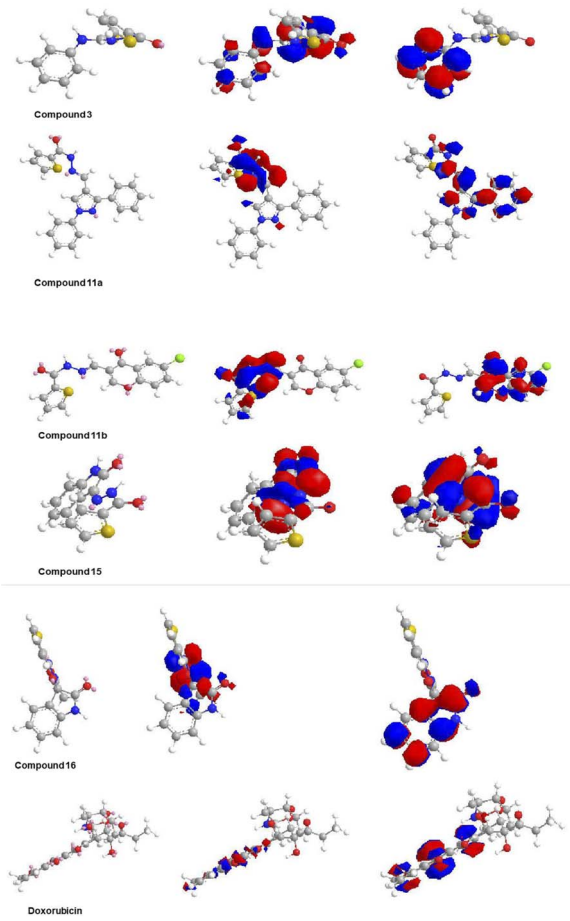


Fig. 3 Optimized structures (left), HOMO (middle), and LUMO (right) for compounds **3–18**. Atom color index: grey C, white H, blue N, red O, yellow S, and green Cl (see all compounds in the ESI†).

Table 2 *In vitro* cytotoxic activity of the tested compounds against tumor cell lines

| | *In vitro* cytotoxicity $IC_{50}$[a] (μM) ± S.D. | |
|---|---|---|
| Compound | MCF7 | HCT116 |
| **3** | 25.18 ± 4.3 | 33.11 ± 3.1 |
| **4** | 52.15 ± 3.9 | 45.20 ± 2.1 |
| **6** | 73.20 ± 4.8 | 54.07 ± 3.8 |
| **7** | 28.53 ± 1.8 | 37.81 ± 1.5 |
| **8** | 45.44 ± 3.0 | 40.24 ± 2.7 |
| **11a** | 11.36 ± 2.5 | 10.82 ± 2.3 |
| **11b** | 6.55 ± 0.4 | 8.20 ± 0.5 |
| **14** | 48.52 ± 1.7 | 39.84 ± 1.6 |
| **15** | 9.35 ± 2.4 | 8.76 ± 2.3 |
| **16** | 15.25 ± 2.6 | 17.75 ± 2.7 |
| **17** | 39.57 ± 1.9 | 27.89 ± 1.4 |
| **18** | 46.44 ± 3.5 | 39.63 ± 1.9 |
| Doxorubicin | 4.17 ± 0.3 | 5.23 ± 0.3 |

[a] $IC_{50}$ (μM): 1–10 (very strong), 11–20 (strong), 21–50 (moderate), 51–100 (weak), and >100 (non-cytotoxic). S.D.: standard deviation.

implications for how to choose a reliable exchange-correlation functional in the computational solvents and catalyst on reactant surface.

Quantum chemical parameters calculations with DFT method used for the calculations of the synthesized compounds are in good agreement with the anticancer efficiency (Table 1). The results pointed at that the values of gap energy ($\Delta E$), where $\Delta E = E_{LUMO} - E_{HOMO}$, follow the order: doxorubicin < **11b** < **15** < **11a** < **6** < **14** < **18** < **4** < **17** < **3** < **16** < **7** < **8**. Compounds having small $\Delta E$ values are generally referred to as soft compounds, that are more reactive towards radical surface interactions; being efficient of donating electrons easily to hole surface. Thus, compound **11b** exhibited the lowest $\Delta E$ value (3.127 eV) compared to the other compounds. Chemical softness values decrease in the order of **11b**, **15**, **11a**, and **16**, respectively, while the hardness values increase in the same order.

The scavenging ability toward positive hole, tumor, radical, and oxygen removable not only depended upon $E_{HOMO}$ values but also, the number of heteroatoms, electron distributions, surface area, and lipophilicity should be considered. The dipole moment (Debye), and softness ($\sigma$, $eV^{-1}$), for most potent compounds holding hydrophobic groups were agreed to an outstanding correlation between oxidation inhibition efficiencies. Correspondingly, compounds of higher binding energy are of higher potency due to the strong interaction between these compounds and the receptors' active sites.

### Biology

***In vitro* antiproliferative activity.** The *in vitro* antiproliferative activity of produced substances was examined against breast adenocarcinoma (MCF7) and colon cancer (HCT116) cell lines utilizing doxorubicin as a standard anticancer agent by MTT assay and was expressed as inhibition concentration fifty ($IC_{50}$) values in μM.[39] The MTT assay is a standard colorimetric assay for measuring cell growth. It is utilized to determine cytotoxicity of potential medicinal agents and other toxic materials. The results in Table 2 and Fig. 4 displayed that the investigated compounds disclosed variable inhibitory activity from high to poor effect. The most active compound **11b** exhibited $IC_{50}$ values of 6.55 and 8.20 μM against breast and colon cell lines, respectively, a potency can be defined very high in the nanomolar range. In turn, compound **15** showed $IC_{50}$ values of 9.35 and 8.76 μM, compound **11a** exhibited $IC_{50}$ values of 11.36 and 10.82 μM, and spiro compound **16** displayed $IC_{50}$ values of 15.25 and 17.75 μM, respectively compared to the reference, doxorubicin with $IC_{50}$ values of 4.17 and 5.23 μM. Most of the compounds showed weak or moderate antiproliferative activity.

## Structure–activity relationship (SAR)

The inhibitory activity of the tested compounds may perhaps be correlated to structure variation and modifications. The produced thiophene derivatives with sided electron-withdrawing head play a substantial role in the binding interactions with receptor subsites *via* van der Waals interaction and hydrogen bonding, as well, facilitate pi-stacking interactions of the loop C aromatic residue with the side chain. The presence of aromatic scaffold in these compounds increased hydrophobicity which improves their permeability into the cell membrane, therefore increasing the antiproliferative activity. The presence of nitrogen atoms allows to improve solubility. Also, the analogs with extended conjugation had higher affinity to form a face-to-edge aromatic interaction with the receptor. Accordingly, it was revealed that the chromone scaffold in hydrazone **11b** pyrazole core in hydrazone **11a** increased the inhibitory effect against the cell lines which may be attributable to the formation of hydrogen bonding with receptor. The existence of indolin-2-one core (as in compound **15**) enhanced its biological profile. The presence of spiro-indolin-oxadiazole

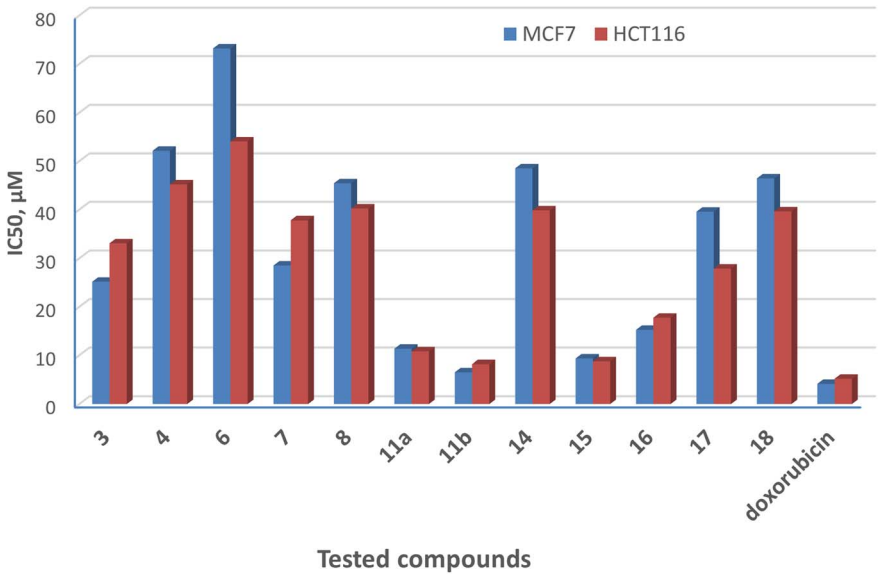


Fig. 4 $IC_{50}$ values of the tested compounds against MCF7 and HCT116 cell lines.

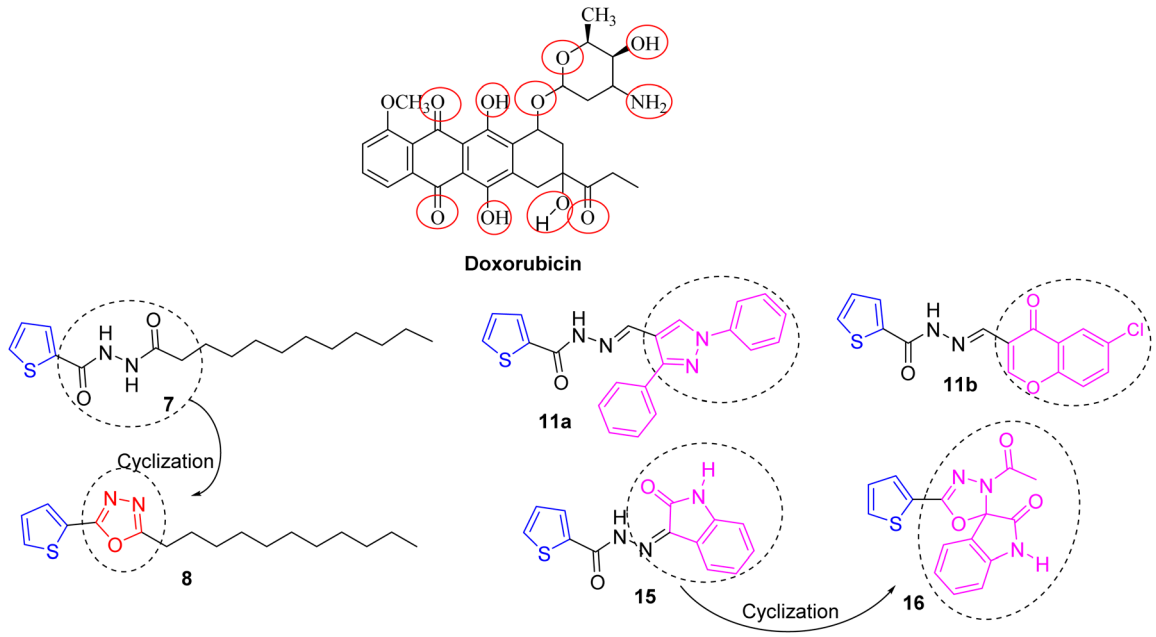


Fig. 5 SAR of compounds 7, 8, 11a, 11b, 15, and 16.

cores (as in compound **16**) boosted the activity *via* extra hydrogen bonding with the receptor active sites. Cyclization of side chain to oxadiazole core (as in compound **8**) strongly reduced the cytotoxic potency (*cf.* Fig. 5).

## Molecular docking study

A molecular docking study was conducted utilizing molecular operating environment (MOE 2019.0102) to demonstrate the binding energies of produced substances toward human carbonic anhydrase IX (CA IX) protein (PDB ID: 5FL4) and determine the interactions between the produced ligands and receptors to compare the affinities of produced complexes toward the target binding sites of protein. The binding affinity was recorded by the binding energies (*S*-score, kcal $mol^{-1}$) and hydrogen bonds. All produced complexes were docked in the same groove of binding site of native co-crystallized ligand (9FK) (Table 3, Fig. 6).

As per data presented in Table 3, the binding energies of the ligands are near to that of co-crystallized ligand (9FK). Compound **11b** exhibits binding energy of −5.5817 kcal $mol^{-1}$ with RMSD of 2.0147 Å referring to tightly binding to some key nucleobases and amino acids (THR 200, TRP 9, and THR 200) of CA IX protein revealing its potential usage as DNA intercalator and CA IX inhibitor. In turn, compound **11a** displays a higher binding energy compared to the reference ligand (9FK) with RMSD 1.1713 Å. This suggests that compound **11a** displays a notably strong binding affinity towards the human carbonic anhydrase IX (CA IX) protein, with binding energies recorded at −6.2788 kcal $mol^{-1}$. The lowest RMSD value was shown for compound **15** at 0.8742 Å. Table 3 further outlines the specific amino acids involved in the

Table 3 Binding amino acids in four compounds and a reference ligand to the human carbonic anhydrase IX (CA IX) protein

| Compound | *S*-score (kcal $mol^{-1}$) | RMSD (Å) | Binding amino acids (bond type) | Bond length (Å) |
|---|---|---|---|---|
| **11a** | −6.2788 | 1.1713 | LEU 91 pi-H | 4.52 |
| | | | GLN 92 pi-H | 4.81 |
| | | | VAL 130 pi-H | 4.12 |
| **11b** | −5.5817 | 2.0147 | THR 200 H-donor | 3.18 |
| | | | TRP 9 H-acceptor | 3.07 |
| | | | THR 200 pi-H | 4.61 |
| **15** | −5.5655 | 0.8742 | HIS 94 pi–pi | 3.93 |
| **16** | −5.9094 | 0.8906 | ASN 66 H-donor | 3.28 |
| | | | ASN 66 H-acceptor | 3.11 |
| | | | HIS 68 H-pi | 4.07 |
| Co-crystallized ligand (9FK) | −5.8123 | 1.0832 | HIS 94 H-donor | 3.04 |
| | | | HIS 94 H-acceptor | 3.23 |
| | | | THR 200 H-acceptor | 2.79 |
| | | | LEU 199 pi-H | 3.80 |

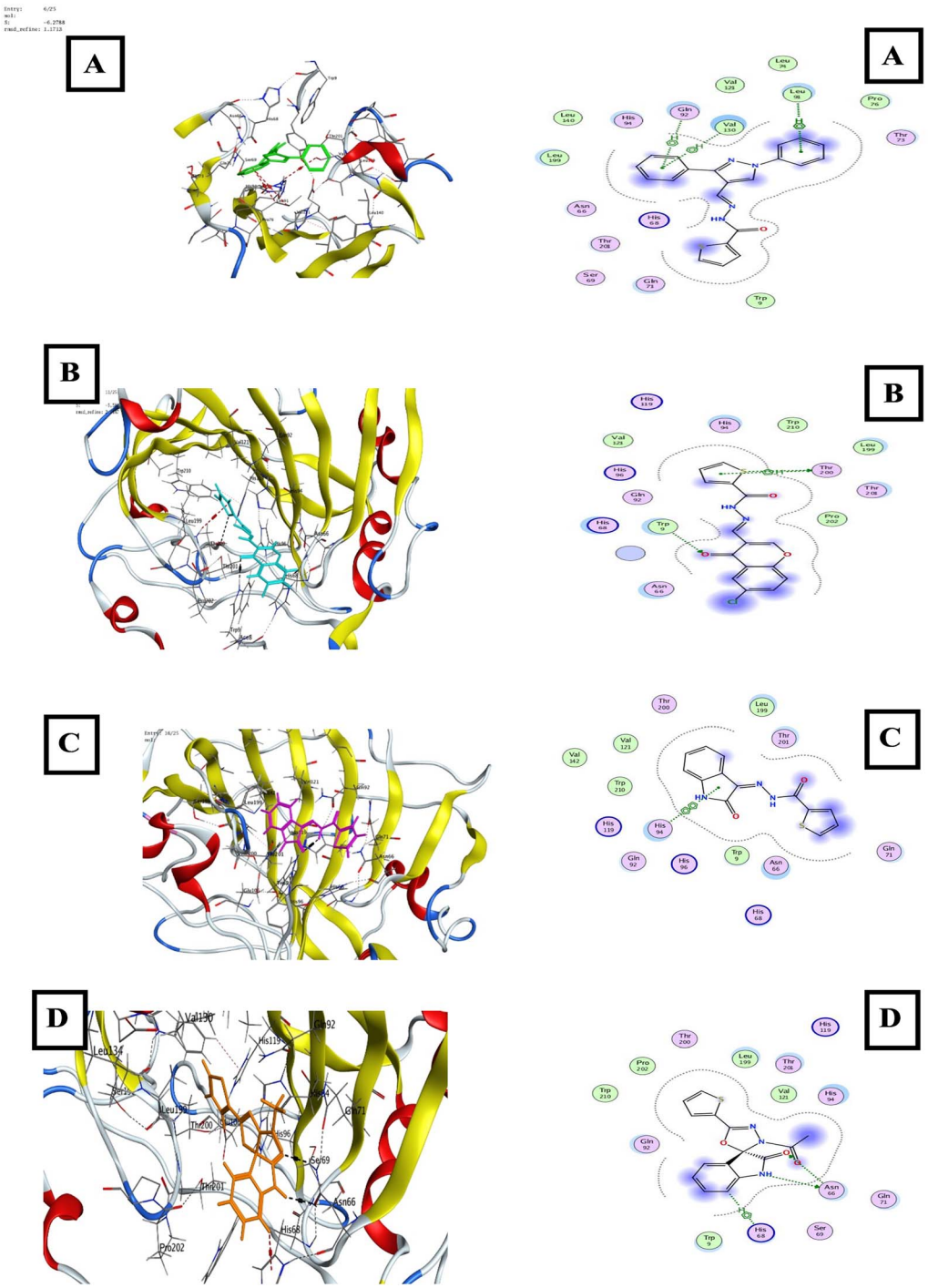


Fig. 6 2D and 3D-interactions of compounds **11a** (A), **11b** (B), **15** (C), and **16** (D) with CA IX protein binding pockets.

binding interaction between each compound and its respective target protein. It provides comprehensive information regarding the binding amino acids and the types of bonds formed, such as H-acceptor, pi-cation, among others, for each compound in association with its respective protein target.

The results of docking analysis of compounds **11a**, **11b**, **15**, and **16** with the human carbonic anhydrase IX (CA IX) protein are depicted in graphical representations (*cf.* Fig. 6), designated as compound **11a** (A), compound **11b** (B), compound **15** (C), and compound **16** (D). In the left panels of Fig. 6, a 3D visualization showcases the binding interactions between these compounds and the CA IX protein, emphasizing hydrogen bonding interactions highlighted in red. Conversely, the right panels present a 2D depiction illustrating detailed insights into the molecular interactions between each of compounds and protein.

## Validation of docking performance and accuracy

To confirm the accuracy of the MOE program, a validation process involved comparing co-crystallized ligands with their respective protein targets. This was achieved by visually overlaying the native co-crystallized ligand (shown in cyan) with the redocked co-crystallized ligand (depicted in red) using 3D diagrams. Root mean square deviation (RMSD) values were calculated for these overlays, and the results were graphically presented, as depicted in Fig. 7. The calculated RMSD value of 1.08 Å quantifies the disparity between these two structures, indicating their level of deviation from each other.

### *In silico* studies

The ADME profiles of the potent compounds, which include their physicochemical properties, lipophilicity, and drug-likeness, have been predicted in order to reduce the time required to choose compounds from a vast collection of compounds in the early stages of drug discovery, biological activities, and development for an effective drug.[40–42] Compounds **11a**, **11b**, **15**, and **16** with a total polar surface area (TPSA) of 87.52, 99.91, 98.80, and 99.24 Å, respectively, and good lipophilicity, as shown by the consensus log $P_{o/w}$ which were in 3.98, 3.04, 1.97, and 2.08, was found to comply with Lipinski's rule of five. According to calculations, they exhibit a high GI absorption and an excellent bioavailability score (0.55), as shown in Table 4.

Their skin permeation ($\log K_P$) parameters were −5.39, −5.98, −6.02, and −6.84 cm $s^{-1}$, which made the bioactive compounds easier to access through the skin. Also, their cytochrome P450 isoenzymes (CYP1A2, CYP2C19, CYP2C9, CYP2D6, and CYP3A4), which play a significant role in the biotransformation of medicines through O-type oxidation processes, have also been predicted (see Table 4). Based on the pink area on the radar chart for compounds (*cf.* Fig. 8–11 in ESI†), the bioavailability of those substances was also calculated. The compounds **11a**, **11b**, **15**, and **16** were fully included in the pink area and this supported their well-predicted oral bioavailability.

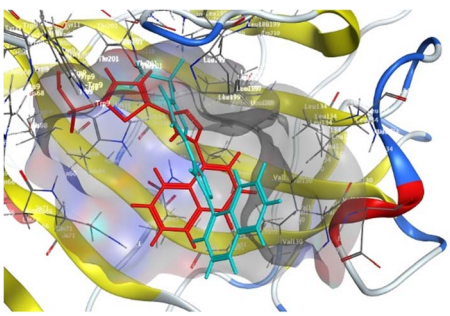

Fig. 7 3D diagram displays the overlay of the native co-crystallized ligand, etoposide (in cyan), with the redocked co-crystallized ligand (in red) within the CA IX protein target.

Table 4 Physicochemical properties/lipophilicity/drug-likeness properties of compounds **11a**, **11b**, **15**, and **16**[a]

| | Compounds | | | |
|---|---|---|---|---|
| Entry | **11a** | **11b** | **15** | **16** |
| Molecular weight (g $mol^{-1}$) | 372.44 | 332.76 | 271.29 | 313.33 |
| Num. heavy atoms | 27 | 22 | 19 | 22 |
| Num. arom. heavy | 22 | 15 | 11 | 11 |
| Fraction $Csp^3$ | 0.00 | 0.00 | 0.00 | 0.13 |
| Num. rotatable bonds | 6 | 4 | 3 | 2 |
| Num. H-bond acceptor | 3 | 4 | 3 | 4 |
| Num. H-bond donors | 1 | 1 | 2 | 1 |
| Molar refractivity | 108.05 | 86.54 | 75.81 | 91.40 |
| TPSA ($Å^2$) | 87.52 | **99.91** | 98.80 | 99.24 |
| Consensus log $P_{o/w}$ | 3.98 | 3.04 | 1.97 | 2.08 |
| Lipinski's rule | **Yes** | **Yes** | **Yes** | **Yes** |
| Bioavailability score | **0.55** | **0.55** | **0.55** | **0.55** |
| **Pharmacokinetics** | | | | |
| GI absorption | High | High | High | High |
| BBB permeant | No | No | No | No |
| P-gp substrate | No | No | No | No |
| CYP1A2 inhibitor | **Yes** | **Yes** | **Yes** | No |
| CYP2C19 inhibitor | **Yes** | **Yes** | **Yes** | No |
| CYP2C9 inhibitor | **Yes** | **Yes** | No | No |
| CYP2D6 inhibitor | No | No | No | No |
| CYP3A4 inhibitor | **Yes** | No | No | No |
| log $K_P$ (skin permeation) (cm $s^{-1}$) | −5.39 | −5.98 | −6.02 | −6.84 |

[a] See more details in the ESI.

## Conclusion

The current study clearly reported the design and synthesis of some thiophene-encompassing heterocycles *via* reactions of thiophene-2-carbohydrazide with some carbon-centered electrophilic reagents. The *in vitro* antiproliferative activity of the synthesized substrates against breast adenocarcinoma (MCF7) and colon cancer (HCT116) cell lines revealed that the most potent compounds were the hydrazone **11b** with $IC_{50}$ values of 6.55 and 8.20 μM and compound **15** with $IC_{50}$ values of 9.35 and 8.76 μM, against breast and colon cell lines, respectively. In turn, compound **11a** exhibited $IC_{50}$ values of 11.36 and 10.82 μM, and spiro compound **16** displayed $IC_{50}$ values of 15.25 and 17.75 μM, respectively. The computational chemical results were consistent with the cytotoxicity of the tested compounds. Thus, compound **11b** exhibited the lowest Δ*E* value (3.127 eV) and the highest softness (0.640 $eV^{-1}$) compared to the other compounds. The molecular docking was conducted to demonstrate the binding energies of produced substances toward human carbonic anhydrase IX (CA IX) protein and determined the interactions between the produced ligands and receptors to compare the affinities of produced complexes toward the target binding sites of protein. The binding energies of these ligands were near to that of co-crystallized ligand (9FK). Compound **11b** exhibits a binding energy of −5.5817 kcal $mol^{-1}$ referring to tightly binding to some key nucleobases and amino acids (THR 200, TRP 9, and THR 200) of CA IX protein revealing its potential

usage as DNA intercalator and CA IX inhibitor. In turn, compound **11a** displays a higher binding energy compared to the reference ligand (9FK). This suggests that compounds **11b** and **11a** display a notably strong binding affinity towards the human carbonic anhydrase IX (CA IX) protein. The modeling pharmacokinetics studies involving physicochemical properties, lipophilicity, and drug-likeness of the strong compounds have been anticipated and revealed that the compounds **11a**, **11b**, **15**, and **16** were fully included in the pink area and this supported their well-predicted oral bioavailability. The most active candidates may serve as useful lead compounds in search of powerful and selective antiproliferative agents. These results are beneficial for additional studies on the advancement of novel and effective anticancer agents.

## Materials and methods

### General

Melting points (°C, uncorrected) were measured on a MEL-TEMP II electric melting point apparatus. The IR spectra were recorded using KBr disks on FTIR Thermo Electron Nicolet 7600 (USA) infrared spectrometer at Faculty of Science, Ain Shams University. The $^1$H NMR spectra were run at 300 MHz on a GEMINI NMR spectrometer using tetramethyl silane (TMS) as internal standard in deuterated dimethyl sulfoxide (DMSO-$d_6$) at Faculty of Science, Cairo University. The $^{13}$C NMR spectra were run at 100 MHz on a BRUKER NMR spectrometer using tetramethyl silane (TMS) as internal standard in deuterated dimethyl sulfoxide (DMSO-$d_6$) at Faculty of Pharmacy, Cairo University. Mass spectra were measured on a Shimadzu GC-MS-QP-1000 EX mass spectrometer running at 70 eV at Faculty of Science, Ain Shams University. The reactions were checked by the thin-layer chromatography using Merck Kiesel gel 60 $F_{254}$ aluminium backed plates. Elemental analyses were recorded at Faculty of Science, Ain Shams University utilizing PerkinElmer 2400 CHN elemental analyser.

***N*-Phenyl-2-(thiophene-2-carbonyl)hydrazine-1-carbothioamide (3).**[33] A solution of thiophene-2-carbohydrazide **1** (0.01 mol) and phenyl isothiocyanate **2** (0.01 mol) in absolute ethanol (20 mL) was refluxed for 1 h. The solid obtained while heating was collected and recrystallized from ethanol/1,4-dioxane (2 : 1) to produce white crystals, mp. 172–174 °C.[33] Yield 91%.

***N*-Phenyl-*N*-(5-(thiophen-2-yl)-1,3,4-oxadiazol-2-yl)glycine (4).** A solution of thiosemicarbazide **3** (1 mmol) and chloroacetic acid (1 mmol) in dimethyl formamide (15 mL) including triethylamine (0.1 mL) was refluxed for 6 h. The solid obtained was collected and recrystallized from 1,4-dioxane to furnish beige crystals, mp. 240–242 °C. Yield 51%. IR ($\nu$, cm$^{-1}$): 3437 (br. OH), 1728 (C=O). $^1$H NMR ($\delta$, ppm): 11.05 (br.s, 1H, OH, exchangeable), 7.91–7.38 (m, 8H, Ar–H), 4.03 (s, 2H, $CH_2$). $^{13}$C NMR ($\delta$, ppm): 43.80, 115.30, 119.71, 122.52, 126.20, 127.51, 129.15, 134.11, 138.46, 143.61, 146.55, 150.23, 161.72, 166.60. EIMS, *m*/*z*, (%): 301.20 ($M^+$, 1), 275.21 ($M^+ - C_2H_2$, 1), 243.13 (2), 165.12 (3), 101.03 (17), 86.04 (100), 58.02 (43). Anal. calcd for $C_{14}H_{11}N_3O_3S$ (301.32): C, 55.81; H, 3.68; N, 13.95; found: C, 55.72; H, 3.61; N, 13.90%.

**Ethyl 2-((4-phenyl-5-(thiophen-2-yl)-4*H*-1,2,4-triazol-3-yl)thio)acetate (6).**[43] A solution of **3** (1 mmol) and ethyl chloroacetate (1 mmol) in glacial acetic acid (20 mL) including anhydrous sodium acetate (1 mmol) was refluxed for 5 h. The reaction mixture was allowed to stand at room temperature, and then poured onto ice-cold water. The solid obtained was collected, dried, and crystallized from ethanol to furnish colorless needles, mp. 134–136 °C.[43] Yield 68%. IR ($\nu$, cm$^{-1}$): 1736 (C=O). $^1$H NMR ($\delta$, ppm): 7.95–7.41 (m, 8H, Ar–H), 4.90 (s, 2H, $CH_2$), 4.15 (q, 2H, $CH_3C\underline{H}_2$, $J = 6.5$ Hz), 1.21 (t, 3H, $CH_2C\underline{H}_3$, $J = 6.5$ Hz). EIMS, *m*/*z*, (%): 345.41 ($M^+$, 37), 272.30 ($M^+ - COOC_2H_5$, 49), 186.42 (26), 135.03 (23), 110.21 (30), 107.03 (14), 77.02 (100). Anal. calcd for $C_{16}H_{15}N_3O_2S_2$ (345.44): C, 55.63; H, 4.38; N, 12.16; found: C, 55.56; H, 4.29; N, 12.20%.

***N*′-Dodecanoylthiophene-2-carbohydrazide (7).**[44] A solution of thiophene-2-carbohydrazide **1** (1 mmol) and dodecanoyl chloride (1.1 mmol) in pyridine (5 mL) was heated in a water bath at ~90 °C for 6 h. The reaction mixture was cooled to room temperature and then poured onto ice/HCl while stirring. The solid obtained was collected, dried, and crystallized from petroleum ether (80–100) to furnish beige crystals, mp. 100–102 °C,[44] yield 78%.

**2-(Thiophen-2-yl)-5-undecyl-1,3,4-oxadiazole (8).** A suspension of hydrazide **7** (1 mmol) in phosphorus oxychloride (10 mL) was heated on a water bath at ~70 °C for 6 h. The reaction mixture was cooled to room temperature and then poured onto ice-cold water. The solid obtained was collected, dried, and crystallized from ethanol to offer beige crystals, mp. 142–144 °C, yield 67%. IR ($\nu$, cm$^{-1}$): 2955, 2921, 2849 (Aliph-CH), 1599 (C=N). $^1$H NMR ($\delta$, ppm): 7.84–7.80 (m, 2H, Ar–H), 7.16 (d, 1H, Ar–H, $J = 7.8$ Hz), 2.15 (t, 2H, $CH_2$, $J = 6.5$ Hz), 1.56–1.50 (m, 2H, $CH_2$), 1.20–1.14 (m, 16H, 8 $CH_2$), 0.85 (t, 3H, $CH_3$, $J = 6.8$ Hz). EIMS, *m*/*z*, (%): 306.10 ($M^+$, 9), 280.15 (15), 223.20 (13), 178.03 (20), 165.02 (17), 155.11 (27), 113.10 (24), 83.03 (100). Anal. calcd for $C_{17}H_{26}N_2OS$ (306.47): C, 66.63; H, 8.55; N, 9.14; found: C, 66.55; H, 8.48; N, 9.18%.

**Synthesis of hydrazones 11a and 11b.** Method I: A solution of hydrazide **1** (1 mmol) and arylidine malononitrile namely, 2-((1,3-diphenylpyrazol-4-yl)methylene)malononitrile (**9a**), or 2-((6-chloro-4-oxochromen-3-yl)methylene)malononitrile (**9b**) in 1,4-dioxane (20 mL) was refluxed for ~8 h. The solid obtained after cooling was collected and crystallized from the appropriate solvent to achieve the hydrazones **11a** and **11b**, respectively.

Method II: A solution of hydrazide **1** (1 mmol) and heterocyclic aldehydes namely, 1,3-diphenylpyrazole-4-carbaldehyde (**12a**), or 6-chloro-4-oxochromene-3-carbaldehyde (**12b**) (1 mmol) in absolute ethanol (20 mL) was refluxed for 3 h. The precipitated solid while heating was collected and crystallized from the appropriate solvent to achieve the hydrazones **11a** and **11b**, respectively.

***N*′-((1,3-Diphenyl-1*H*-pyrazol-4-yl)methylene)thiophene-2-carbohydrazide (11a).**[34a] Yellow crystals, mp. 250–252 °C (ethanol/1,4-dioxane, 2 : 1). Yield 87%. IR ($\nu$, cm$^{-1}$): 3282 (NH), 1649 (C=O). $^1$H NMR ($\delta$, ppm): 11.70 (br.s, 1H, NH, exchangeable), 8.98 (s, 1H, CH=N), 8.54 (s, 1H, C5–H pyrazole), 8.03–7.20 (m, 13H, Ar–H). EIMS, *m*/*z* (%): 372.3 ($M^+$, 10), 245.2 (100),

244.2 (26), 127.0 (14), 111.4 (99), 104.2 (10), 77.2 (59), 76.3 (15). Anal. calcd for $C_{21}H_{16}N_4OS$ (372.45): C, 67.72; H, 4.33; N, 15.04; found: C, 67.65; H, 4.29; N, 15.06%.

***N*′-((6-Chloro-4-oxo-4*H*-chromen-3-yl)methylene)thiophene-2-carbohydrazide (11b).**[34b] Beige crystals, mp. 232–234 °C (ethanol).[34b] Yield 84%.

**2-(1*H*-Indol-3-yl)-5-(thiophen-2-yl)-1,3,4-oxadiazole (14).** A solution of hydrazide **1** (1 mmol) and 3-formylindole (1 mmol) in 1,4-dioxane (10 mL) was refluxed for 8 h. The solid obtained was collected and crystallized from 1,4-dioxane to produce yellow crystals, mp. 270–272 °C, yield 53%. IR ($\nu$, $cm^{-1}$): 3215 (NH), 1626 (C=N). $^1H$ NMR ($\delta$, ppm): 11.41 (br.s, 1H, NH, exchangeable), 8.61 (s, 1H, C2–H indole), 8.29 (t, 1H, Ar–H, $J$ = 7.8 Hz), 7.94–7.81 (m, 2H, Ar–H), 7.45 (d, 1H, Ar–H, $J$ = 7.5 Hz), 7.21–7.13 (m, 3H, Ar–H). Anal. calcd for $C_{14}H_9N_3OS$ (267.31): C, 62.91; H, 3.39; N, 15.72; found: C, 62.83; H, 3.32; N, 15.75%.

***N*′-(2-Oxoindolin-3-ylidene)thiophene-2-carbohydrazide (15).**[35] A solution of hydrazide **1** (1 mmol) and indolin-2,3-dione (1 mmol) in ethanol (20 mL) was refluxed for 2 h. The solid obtained while heating was collected and recrystallized from ethanol/1,4-dioxane mixture (2 : 1) to afford yellow crystals, mp. 248–250 °C.[35]

**3′-Acetyl-5′-(thiophen-2-yl)-3′*H*-spiro[indoline-3,2′-[1,3,4]oxadiazol]-2-one (16).** A suspension of **16** (1 mmol) in acetic anhydride (10 mL) was refluxed for 5 h. The reaction mixture was concentrated. After cooling, the solid obtained was collected and recrystallized from ethanol to give yellow crystals, mp. 178–180 °C, yield 59%. IR ($\nu$, $cm^{-1}$): 3228 (NH), 1714 (C=O indolinone), 1663 (amide), 1649 (C=N). $^1H$ NMR ($\delta$, ppm): 12.80 (br.s, 1H, NH, exchangeable), 8.14 (d, 1H, Ar–H, $J$ = 8.0 Hz), 8.07–7.99 (m, 2H, Ar–H), 7.75 (d, 1H, Ar–H, $J$ = 7.5 Hz), 7.52 (t, 1H, Ar–H, $J$ = 7.3 Hz), 7.37–7.29 (m, 2H, Ar–H), 2.64 (s, 3H, $CH_3$). $^{13}C$ NMR ($\delta$, ppm): 30.41, 115.30, 119.72, 122.21, 126.13, 127.95, 128.97, 129.53, 130.11, 135.44, 138.55, 141.30, 144.40, 161.21, 162.20. Anal. calcd for $C_{15}H_{11}N_3O_3S$ (313.33): C, 57.50; H, 3.54; N, 13.41; found: C, 57.39; H, 3.47; N, 13.38%.

***N*-(2-(1,3-Diphenyl-1*H*-pyrazol-4-yl)-4-oxothiazolidin-3-yl)thiophene-2-carboxamide (17).** A mixture of hydrazone **11a** (1 mmol) and mercaptoacetic acid (1 mmol) was fused in a sand bath at 130–140 °C for 2 h. After cooling, the reaction mixture was poured on 10% sodium carbonate solution and left overnight. The solid obtained was collected, dried, and crystallized from benzene to give yellow crystals, mp. 148–150 °C, yield 57%. IR ($\nu$, $cm^{-1}$): 3226 (NH), 1710, 1680 (C=O). $^1H$ NMR ($\delta$, ppm): 8.79 (br.s, 1H, NH, exchangeable), 8.70 (s, 1H, C5–H pyrazole), 8.01–7.36 (m, 13H, Ar–H), 6.01 (s, 1H, C2–H thiazolidinone), 3.85 (d, 1H, 1H of $CH_2$, $J$ = 7.0 Hz), 3.75 (d, 1H, 1H of $CH_2$, $J$ = 7.0 Hz). $^{13}C$ NMR ($\delta$, ppm): 42.50, 60.30, 115.66, 118.77, 119.88, 123.14, 126.90, 128.10 (3), 128.60, 128.89 (3), 131.48, 132.32, 133.98, 134.15, 138.48, 141.20, 161.96, 164.99, 165.80. EIMS, $m/z$ (%): 446.01 ($M^+$, 1) 432.11 (4), 429.60 ($M^+$ − OH, 5), 320.23 (34), 319.22 (24), 263.41 (32), 246.21 (20), 162.32 (11), 143.02 (14), 122.13 (15), 110.71 (35), 105.22 (49), 77.11 (100), 51.10 (43). Anal. calcd for $C_{23}H_{18}N_4O_2S_2$ (446.54): C, 61.86; H, 4.06; N, 12.55; found: C, 61.72; H, 3.99; N, 12.51%.

**1-(2-(1,3-Diphenyl-1*H*-pyrazol-4-yl)-5-(thiophen-2-yl)-1,3,4-oxadiazol-3(2*H*)-yl)ethan-1-one (18).** A suspension of hydrazone **11a** (1 mmol) in acetic anhydride (10 mL) was refluxed for 4 h. The reaction mixture was left overnight. The solid obtained was filtered off and crystallized from light petroleum ether/benzene to give yellow crystals, mp. 208–210 °C, yield 64%. IR ($\nu$, $cm^{-1}$): 1650 (C=O), 1626 (C=N). $^1H$ NMR ($\delta$, ppm): 8.79 (s, 1H, C5–H pyrazole), 7.95–7.32 (m, 13H, Ar–H), 7.25 (s, 1H, C2–H oxadiazole), 2.21 (s, 3H, $CH_3$). EIMS, $m/z$ (%): 414.21 ($M^+$, 11), 377.12 (30), 334.32 (17), 301.21 (100), 292.13 (26), 250.30 (60), 247.21 (27), 166.21 (9), 110.32 (18), 77.01 (28). Anal. calcd for $C_{23}H_{18}N_4O_2S$ (414.48): C, 66.65; H, 4.38; N, 13.52; found: C, 66.57; H, 4.32; N, 13.55%.

### *In vitro* antiproliferative assay

**Cell lines.** Cytotoxic activity of compounds obtained was examined against two cell lines namely, breast cancer (MCF7) and colon cancer (HCT116), obtained from the ATCC through the Holding Company for Biological Products and Vaccines (VACSERA, Cairo, Egypt).

**Chemical reagents.** The reagents RPMI-1640 medium, MTT, and DMSO (Sigma Co., St. Louis, USA), Fetal Bovine serum (GIBCO, UK). Doxorubicin was utilized as a standard anticancer agent for comparison.

**MTT assay.** The two cell lines were utilized to evaluate the inhibitory effects of compounds on cell growth using the MTT assay.[39] This colorimetric assay was based on the conversion of the yellow tetrazolium bromide (MTT) to a purple formazan derivative by mitochondrial succinate dehydrogenase in viable cells. The cells were cultured in RPMI-1640 medium with 10% fetal bovine serum. Antibiotics added were 100 units per mL penicillin and 100 μg per mL streptomycin at 37 °C in a 5% $CO_2$ incubator. The cells were seeded in a 96-well plate at a density of $1.0 \times 10^4$ cells per well at 37 °C for 48 h under 5% $CO_2$. After incubation, the cells were treated with different concentrations of compounds and incubated for 24 h. After 24 h of agent treatment, 20 μL of MTT solution at 5 mg $mL^{-1}$ were added and incubated for 4 h. Carrier solvent, DMSO was used as a negative control, and was added in a volume of 100 μL into each cell to dissolve the purple formazan formed. The colorimetric assay was recorded at the absorbance of 570 nm using a plate reader (EXL 800, USA). The relative cell viability in percentage was calculated as ($A_{570}$ of treated samples/$A_{570}$ of the untreated sample) × 100.

**Molecular docking.** The study employed Molecular Operating Environment (MOE 2019) software to simulate how promising compounds (**11a**, **11b**, **15**, and **16**) interacted and bound with the human carbonic anhydrase IX (CA IX) protein. To begin, the 3D structures of the CA IX proteins were pre-processed using MOE, involving steps such as removing water molecules, eliminating repeating chains, adding protons, and performing energy minimization to refine the protein structures. Subsequently, the binding site was isolated and verified by accurately redocking the original ligands from their respective PDB IDs (*e.g.*, 5FL4), resulting in a root mean square deviation (RMSD) of less than 1.5, ensuring structural validity.

The promising compounds (**11a**, **11b**, **15**, and **16**) were prepared for docking within MOE through the software's

 

chemical structure creation process. Protons were incorporated into the compounds' 3D structures, followed by further energy minimization using the Force Field MMFF94x. These optimized structures were then integrated into the MOE database. The newly synthesized compounds underwent docking simulations within MOE, allowing the determination of their binding energies and elucidation of their binding mechanisms based on the outlined procedures.[45]

## Conflicts of interest

The authors declare that there is no conflict of interest.

## Acknowledgements

The authors extend their appreciation to the Deanship of Scientific Research at King Khalid University for funding this work through the large group Research Project under grant number (RGP2/413/44).

## References

1 P. M. Rademacher, C. M. Woods, Q. Huang, G. D. Szklarz and S. D. Nelson, *Chem. Res. Toxicol.*, 2012, **25**, 895.
2 A. Archna, S. Pathania and P. A. Chawla, *Bioorg. Chem.*, 2020, **101**, 104026.
3 R. Shah and P. K. Verma, *Chem. Cent. J.*, 2018, **12**, 137.
4 M. S. Al-Said, M. S. Bashandy, S. I. Al-qasoumi and M. M. Ghorab, *Eur. J. Med. Chem.*, 2011, **46**(1), 137.
5 K. C. Gulipalli, S. Bodige, P. Ravula, S. Endoori, G. R. Vanaja, B. G. Suresh, J. N. Narendra and N. Seelam, *Bioorg. Med. Chem. Lett.*, 2017, **27**(15), 3558.
6 J. F. de Oliveira, A. L. da Silva, D. B. Vendramini-Costa, C. A. da Cruz Amorim, J. F. Campos, A. G. Ribeiro, R. O. de Moura, J. L. Neves, A. L. T. Gois Ruiz, J. E. de Carvalho and M. C. A. de Lima, *Eur. J. Med. Chem.*, 2015, **104**, 148.
7 A. I. Hashem, W. S. I. Abou-Elmagd, A. K. El-Ziaty and S. K. Ramadan, *J. Heterocycl. Chem.*, 2017, **54**(6), 3711.
8 A. M. Abdelrahman, A. A. Fahmi, S. A. Rizk and E. A. E. El-Helw, *Polycyclic Aromat. Compd.*, 2023, **43**(1), 721.
9 A. I. Hassaballah, S. K. Ramadan, S. A. Rizk, E. A. E. El-Helw and S. S. Abdelwahab, *Polycyclic Aromat. Compd.*, 2023, **43**(4), 2973.
10 E. A. E. El-Helw, A. M. Abdelrahman, A. A. Fahmi and S. A. Rizk, *Polycyclic Aromat. Compd.*, 2023, **43**(9), 8265.
11 L. F. Friesen, A. G. Nelson and R. C. Van Acker, *Agron. J.*, 2003, **95**, 1342.
12 R. Fischer, N. Lui, S. Dutzmann, and G. Haenssler, *Ger. Offen. Pat.*, 19649093, 1998trans*Chem. Abstr.* 1998, 129, P24482.
13 J. W. Pratt, in *Ullmann's Encyclopedia of Industrial Chemistry*, Wiley-VCH, Weinheim, 2003, vol. 36, p. 653.
14 S. K. Ramadan and H. A. Sallam, *J. Heterocycl. Chem.*, 2018, **55**(8), 1942.
15 M. Asran, E. A. E. El-Helw, M. E. Azab, S. K. Ramadan and M. H. Helal, *J. Iran. Chem. Soc.*, 2023, **20**(12), 3023.
16 D. Carbone, C. Pecoraro, G. Panzeca, G. Xu, M. S. Roeten, S. Cascioferro, E. Giovannetti, P. Diana and B. Parrino, *Mar. Drugs*, 2023, **21**(7), 412.
17 A. Türe, M. Ergül, M. Ergül, *et al.*, *Mol. Diversity*, 2021, **25**, 1025.
18 C. Pecoraro, D. Carbone, D. Aiello and A. Carbone, *Arkivoc*, 2022, **2**, 30.
19 A. A. El-Badawy, A. S. Elgubbi and E. A. E. El-Helw, *J. Sulfur Chem.*, 2021, **42**(3), 295.
20 H. Lai, D. Dou, S. Aravapalli, T. Teramoto, G. H. Lushington, T. M. Mwania, K. R. Alliston, D. M. Eichhorn, R. Padmanabhan and W. C. Groutas, *Bioorg. Med. Chem.*, 2013, **21**, 102.
21 A. C. Tripathi, S. J. Gupta, G. N. Fatima, P. K. Sonar, A. Verma and S. K. Saraf, *Eur. J. Med. Chem.*, 2014, **72**, 52.
22 D. Carbone, B. Parrino, S. Cascioferro, C. Pecoraro, E. Giovannetti, V. D. Sarno, S. Musella, G. Auriemma, G. Cirrincione and P. Diana, *ChemMedChem*, 2021, **16**(3), 537.
23 K. N. Halim, S. A. Rizk, M. A. El-Hashash and S. K. Ramadan, *J. Heterocycl. Chem.*, 2021, **58**(2), 636.
24 M. M. Kaddah, A. A. Fahmi, M. M. Kamel, S. K. Ramadan and S. A. Rizk, *Synth. Commun.*, 2021, **51**(12), 1798.
25 S. K. Ramadan, A. K. El-Ziaty and E. A. E. El-Helw, *Synth. Commun.*, 2021, **51**(8), 1272.
26 S. K. Ramadan, N. A. Ibrahim, S. A. El-Kaed and E. A. E. El-Helw, *J. Sulfur Chem.*, 2021, **42**(5), 529.
27 S. K. Ramadan, D. R. Abdel Haleem, H. S. M. Abd-Rabboh, N. M. Gad, W. S. I. Abou-Elmagd and D. S. Haneen, *RSC Adv.*, 2022, **12**(22), 13628.
28 M. M. Kaddah, A. R. Morsy, A. A. Fahmi, M. M. Elsafty, S. A. Rizk and S. K. Ramadan, *Synth. Commun.*, 2021, **51**(22), 3366.
29 N. M. Gad, W. S. I. Abou-Elmagd, D. S. Haneen and S. K. Ramadan, *Synth. Commun.*, 2021, **51**(9), 1384.
30 M. M. Kaddah, A. A. Fahmi, M. M. Kamel, S. A. Rizk and S. K. Ramadan, *Polycyclic Aromat. Compd.*, 2023, **43**(5), 4231.
31 J. L. Abernethy, D. Srulevitch and M. J. Ordway, *J. Org. Chem.*, 1975, **40**, 3445.
32 E. A. E. El-Helw, A. Y. A. Alzahrani and S. K. Ramadan, *Future Med. Chem.*, 2024, DOI: **10.4155/fmc-2023-0304**.
33 A. Siwek, M. Wujec, M. Dobosz, E. Jagiello-Wojtowicz, A. Kleinrok, A. Chodkowska and P. Paneth, *Phosphorus, Sulfur Silicon Relat. Elem.*, 2008, **183**, 2669.
34 (*a*) K. S. Neethu, J. Eswaran, M. Theetharappan, S. P. Bhuvanesh Nattamai, M. A. Neelakantan and K. M. Velusamy, *Appl. Organomet. Chem.*, 2019, **33**(3), e4751; (*b*) M. B. Ismail, I. N. Booysen, M. P. Akerman and C. Grimmer, *J. Organomet. Chem.*, 2017, **833**(15), 18.
35 M. C. Rodríguez-Argüelles, R. Cao, A. M. García-Deibe, C. Pelizzi, J. Sanmartín-Matalobos and F. Zani, *Polyhedron*, 2009, **28**(11), 2187.
36 M. A. Hamza, S. A. Rizk, E.-E. M. Ezz-Elregal, S. A. Abd El-Rahman, S. K. Ramadan and Z. M. Abou-Gamra, *Sci. Rep.*, 2023, **13**(1), 12929.
37 S. K. Ramadan, H. S. Abd-Rabboh, N. M. Gad, W. S. I. Abou-Elmagd and D. S. Haneen, *Polycyclic Aromat. Compd.*, 2023, **43**(8), 7013.

38 S. K. Ramadan and S. A. Rizk, *J. Iran. Chem. Soc.*, 2022, **19**(1), 187.
39 T. Mosmann, *J. Immunol. Methods*, 1983, **65**, 55.
40 A. Daina, O. Michielin and V. Zoete, *Sci. Rep.*, 2017, **7**, 42717.
41 A. Daina and V. Zoete, *ChemMedChem*, 2016, **11**(11), 1117.
42 A. El-Sewedy, E. A. El-Bordany, N. F. H. Mahmoud, K. A. Ali and S. K. Ramadan, *Sci. Rep.*, 2023, **13**(1), 17869.
43 I. F. Nassar, S. R. Att-Allah and M. M. Hemdan, *Phosphorus, Sulfur Silicon Relat. Elem.*, 2018, **193**(10), 630.
44 **https://patents.google.com/patent/US20040063765A1**.
45 H. A. Khatab, S. F. Hammad, E. M. El-Fakharany, A. I. Hashem and E. A. E. El-Helw, *Sci. Rep.*, 2023, **13**(1), 15093.